Journal of Materials Chemistry A

Accepted Manuscript

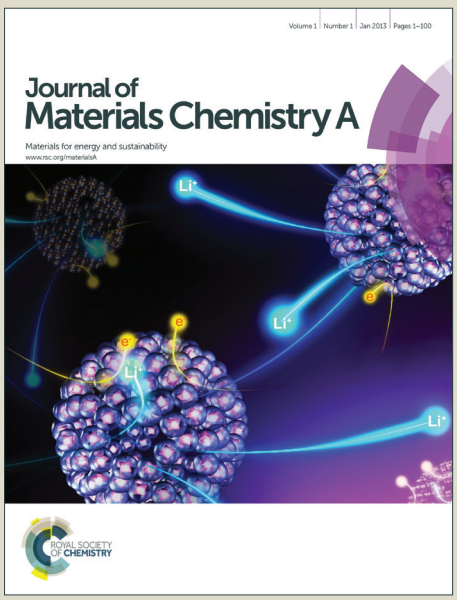

ROYAL SOCIETY OF CHEMISTRY

www.rsc.org/materialsA

Journal of Materials Chemistry A

Cite this: DOI: 10.1039/c0xx00000x

ARTICLE TYPE

www.rsc.org/xxxxxx

A novel activating strategy to achieve highly porous carbon monolith for CO_2 capture

Xiaoyu Ma, Yao Li, Minhua Cao* and Changwen Hu*

Received (in XXX, XXX) Xth XXXXXXXXX 20XX, Accepted Xth XXXXXXXXX 20XX

DOI: 10.1039/b000000x

Highly porous N-doped carbon monolith has been successfully prepared by using binary H_3PO_4-HNO_3 mixed acid as a co-activating agent for the first time and sodium alginate (SA), a natural biopolymer, as carbon precursor. The resultant N-doped carbon monolith has a narrow size distribution and high content of pyrrolic N. Particularly, the sample SA-2N-P with the highest surface area (1740 m^2 g^{-1}) exhibits the highest CO_2 adsorption capacity of 8.99 mmol g^{-1} at 273 K and 4.57 mmol g^{-1} at 298 K, along with an initial CO_2 adsorption energy of 43 kJ mol^{-1} at lower CO_2 coverage and 32 kJ mol^{-1} at higher CO_2 coverage. Remarkably, this sample also shows the highest CO_2 capacity [66.44 mg (CO_2)/g (adsorbent) at 25 °C and 0.15 atm] under low CO_2 pressures, which is of more relevance for flue gas applications. Furthermore, the selectivity of CO_2 over N_2 is also calculated for binary gas mixture [V (N_2): V (CO_2) = 85:15] according to ideal adsorbed solution theory (IAST). Combined with its simple preparation, high adsorption capacity, and high selectivity for CO_2, the sample SA-2N-P is one of the promising solid-state absorbents reported so far for CO_2 capture and storage.

1. Introduction

Carbon dioxide (CO_2), a greenhouse gas presented in the atmosphere, is the biggest contributor to global warming.[1] Therefore, CO_2 capture and storage (CCS) is a promising route to achieve a meaningful reduction in CO_2 emissions from large point sources such as power plants in the near to medium term. The Intergovernmental Panel on Climate Change (IPCC) estimates that CO_2 emissions to the atmosphere could be reduced by 80–90% for a modern conventional power plant equipped with carbon capture and storage technology.[2,3] CO_2 capture and storage technologies mainly include post-combustion (predominantly CO_2/N_2 separation), pre-combustion (CO_2/H_2) capture, and natural gas sweetening (CO_2/CH_4).[2] Post-combustion CO_2 capture (PCCC) technology has the potential to contribute significantly to the reduction of anthropogenic CO_2 emissions from flue gas streams, however the low pressure of the flue gas (*ca*. 1 atm) is its major obstacle. Moreover, the CO_2 concentration in the flue gas is as low as *ca*. 15%, and therefore the capture can only be achieved from a high volume stream of flue gas containing other component gases, predominantly N_2.

Post-combustion capture of CO_2 generally uses various porous solid sorbents such as metal–organic frameworks (MOFs),[4,5] covalent organic frameworks,[6,7] zeolites,[8, 9] porous carbons,[10-13] and amine-functionalized silicas.[14,15] Among these sorbents, carbon materials have more advantages such as low cost, easy decorating and highly chemical, thermal, and mechanical stability, which have been extensively investigated. In recent years, naturally biological materials (such as fungi, celtuce leaves and starch) have been widely used to produce porous carbon materials with novel morphologies.[16-18] These biomasses can be used as very attractive sources for the synthesis of carbon materials due to their low cost, wide availability, and environmental benignity. The porous carbons can be obtained simply by carbonizing these biomasses and then subjecting to further physical or chemical activation. The physical activation mainly consists of etching the carbon materials with oxidative gases (e.g. CO_2, NH_3 and H_2O steam) at high temperatures,[19-21] whereas for the chemical activation process, the carbon precursors are first mixed with activating agents, such as KOH,[22] $ZnCl_2$,[23] or H_3PO_4[24], and followed by pyrolysis. By comparison, the chemical activation allows for obtaining high surface area carbons, which are especially beneficial for the CO_2 adsorption. In order to improve the CO_2 adsorption capacity of porous carbons, a large amount of investigations have been done with special emphasis on developing high surface area microporous carbons and/or incorporating basic species, mainly nitrogen-containing groups into carbon framework.[12, 13]

In this work, we report a facile, large-scale and low-cost strategy to synthesize a series of N-enriched carbon monoliths with high surface area by using sodium alginate (SA) as a green carbon source (extensively used in the food and pharmaceutical industry) and binary acid mixture of H_3PO_4-HNO_3 as a co-

Key Laboratory of Cluster Science, Ministry of Education of China, Beijing Key Laboratory of Photoelectronic/Electrophotonic Conversion Materials, Department of Chemistry, Beijing Institute of Technology, Beijing 100081, P. R. China. E-mail: caomh@bit.edu.cn

† Electronic supplementary information (ESI). See DOI:

activating agent and nitrogen source for the first time. Compared to KOH activating agent, the acid agent can achieve more homogeneous mixing with carbon precursor, which could accelerate this degradation.[25,26] In addition, compared to single H_3PO_4 activation that often results in a rather broad pore distribution,[27] the H_3PO_4-HNO_3 activation can lead to narrower pore distribution of the porous carbons. The direct introduction of heteroatom N in carbons that takes place upon chemical activation with HNO_3-H_3PO_4, offers the potential advantage of avoiding the need for a further functionalization treatment. The "one-step" approach that the synthesis and functionalization are finished synchronously has been scarcely reported to date. The resultant porous carbon monoliths exhibit high CO_2 adsorption capacity. More importantly, they also show high stability and high selectivity for CO_2 over N_2, indicating that these carbon monoliths are candidates for the next generation of CO_2 absorbents. For comparison, SA was directly carbonized in the absence of HNO_3-H_3PO_4 and macroporous carbon was obtained, which is consistent with the reference.[28]

2. Experimental

Synthesis procedures: All chemicals used were analytical grade without further purification. In a typical synthesis, 1.0 g of SA was first dissolved in a mixture of H_3PO_4 and HNO_3 with different doses (V_{HNO_3}:$V_{H_3PO_4}$= 3:0, 2:1, and 1:2) under magnetic stirring at 25 °C for one night to form a milky suspension. Next, an alumina boat with the above suspension was placed in a flow-through tube furnace. The furnace was heated to the required temperature of 750 °C under a nitrogen flow and then maintained at the target temperature for 2 h and cooling down to room temperature. The resulting carbons were refluxed at 90 °C in aqua regia to remove the salt templates. Finally, the as-prepared carbon materials were collected by centrifuging and repeatedly washing by distilled water several times, and finally drying in an oven at 80 °C. Thus a series of samples were obtained and denoted as SA-3N, SA-2N-P and SA-N-2P, respectively. The sample obtained by direct carbonization of SA was denoted as SA.

Characterization: Raman spectra were recorded on an Invia Raman spectrometer, with an excitation laser wavelength of 514.5 nm. The sizes and morphologies of the resulting products were studied by a H-8100 transmission electron microscopy (TEM) operating at 200 kV accelerating voltage. Field emission scanning electron microscopy (FE-SEM) of the sample was taken on Hitachi S-4800 FE-SEM unit. The Brunauer-Emmett-Teller (BET) surface area was measured using a Belsorp-max surface area detecting instrument (Belsorpmax, Bel Japan Inc.,Japan) *via* conventional volumetric technique by Nitrogen adsorption-desorption at 77 K. Pore size distributions (PSDs) were determined from the adsorption branches of the isotherms *via* non local density functional theory (NLDFT) method and assuming a slit pore model. The CO_2 adsorption isotherms were measured at desired temperature using intelligent gravimetric analysis (IGA 003). The instrument was equipped with a thermostat system controlled by a Fisher Scientific isotemp refrigerated circulator. Prior to each adsorption experiment, the sample was first degassed for 3 h at 350 °C and then outgassed at this temperature to a constant vacuum of 10^{-6}-10^{-7} mbar to remove the guest molecules from the pores. A gas stream with the desired composition was passed through the sample, providing good contact between the solid and the adsorbate.

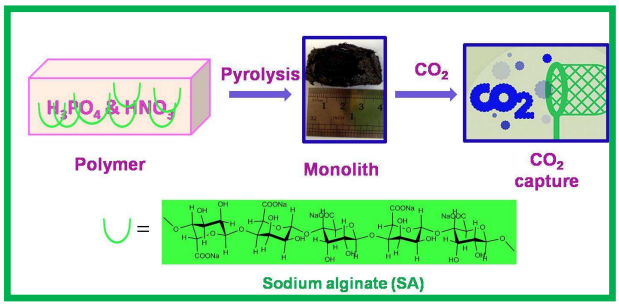

Scheme 1. Schematic illustration of the fabrication of the highly porous carbons.

3. Results and Discussion

Structural properties of the porous carbons

By pyrolyzing HNO_3-H_3PO_4-impregnated SA, a series of samples are synthesized; these samples are denoted as SA-*x*N-*y*P, where *x* and *y* are volumes of HNO_3 and H_3PO_4, respectively (Scheme 1). Raman spectroscopy has been proved to be a powerful, effective tool for carbon materials characterization.[29-31] Fig. 1 shows the Raman spectra of the resultant four samples. It can be clearly seen that all spectra show two typical peaks, which can be attributed to D band at 1350 cm^{-1} and G band at 1600 cm^{-1}, respectively. It has been well addressed that the D band is closely related to the vibration of sp^2-bonded carbon atoms in a two-dimensional hexagonal lattice and the G band is associated with sp^3-hybridized carbon, structural defects, amorphous carbon or edges that can break the symmetry.[29,30,32] As clearly disclosed by Fig. 1, compared to the un-activated SA and the SA-3N activated with only HNO_3, the HNO_3-H_3PO_4 activated samples, SA-2N-P and SA-N-2P, have stronger D band, indicating the fact that these two samples have more defects. These results agree well with that reported by G. L. Cui et al.[29]

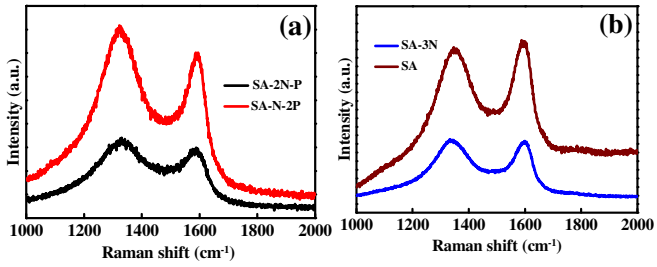

Fig. 1 Raman spectra of the activated carbon materials and un-activated sample.

Figs. 2a-d show field emission scanning electron microscopy (FE-SEM) images of the carbon materials obtained with different activation conditions. It can be clearly seen that these four samples have evident difference in morphology. The HNO_3-H_3PO_4 activated samples, SA-2N-P and SA-N-2P, have similar

morphology. Specifically, the skeleton of carbon monolith consists of homogeneously interconnected spherical units with small size. In contrast, for the sample SA-3N obtained only with HNO_3 as activating agent, it is composed of un-uniform, irregular and large particles (Fig. 3c). Therefore, from this result we can draw the conclusion that the H_3PO_4 used in our experiments acts not only as an activating agent to activate the carbon materials, but also as a capping agent to control the size of particles. This fact has also been proved by many investigations.[24] However,

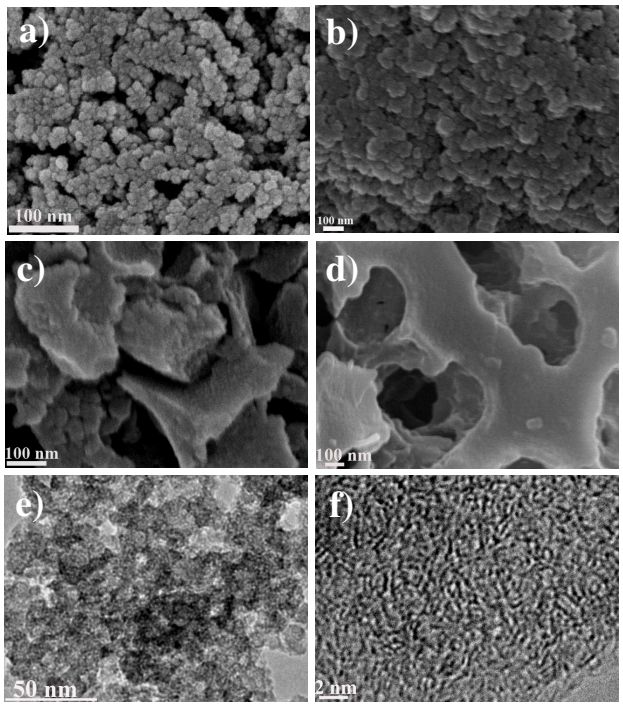

Fig. 2 FE-SEM images of the carbons derived from SA with different activation conditions, (a) SA-2N-P, (b) SA-N-2P, (c) SA-3N, (d) SA. (e) and (f) Low-magnification and high-magnification TEM images of the sample SA-2N-P.

the sample SA changes a lot in morphology compared to other three samples, and it is composed of large agglomerations (>5 μm) with plentiful open cavities with diameter of *ca* 250 nm (Fig. 2d), which result from the removal of *in situ* formed Na_2CO_3 during the pyrolysis process.[28] All of these results clearly indicate that the binary acid mixture of H_3PO_4-HNO_3 plays an important role in the formation of the structure. To further understand the micro-structure and morphology of the sample SA-2N-P, transmission electron microscopy (TEM) measurements were carried out. Fig. 2e further confirms that the sample consists of interconnected spherical particles, which is consistent with above SEM observation. In addition, the disordered slit-like micropores can be clearly seen in a high-resolution transmission electron microscopy (HRTEM) image, as shown in Fig. 2f. This result also indicates that the porosity in this materials results from the micropores distributed all over the skeleton of the microstructures. To understand the effect of the activating agent on the porous characteristics, the nitrogen adsorption-desorption measurements were carried out. The nitrogen sorption isotherms and corresponding pore-size distributions for the four samples are displayed in Fig. 3. For samples SA-2N-P and SA-N-2P, their isotherms are similar and display hysteresis loops at relative pressures close to unity, which can be categorized to type IV according to IUPAC classification,[33] indicating the presence of mesopores. The observed unusual small H3 hysteresis loops indicate that the mesopores belong to the slit-like pores formed through the aggregation of carbon nanoparticles,[34,35] whereas the steep adsorption at low relative pressure ($p/p_0 \approx 0.01$) confirms the presence of abundant micropores. Therefore, it can be concluded that the HNO_3-H_3PO_4 activated samples exhibit a unique microporous–mesoporous hierarchical pore structure. For the sample SA-3N activated with only HNO_3, it exhibits an abundant microporous structure. In contrast, for the sample SA that was not activated, different from above three samples, it does not possess microporous structure. The pore distributions of the four samples are shown in Fig. 3b, which clearly indicate that except for the sample SA, the other three samples exhibit narrow pore distribution mainly in the micropore range. Evidently, the pore distribution in our case depends heavily on the degree of activation to which the carbon materials are subjected. It has been reported that narrow micropores (<1 nm) have a greater

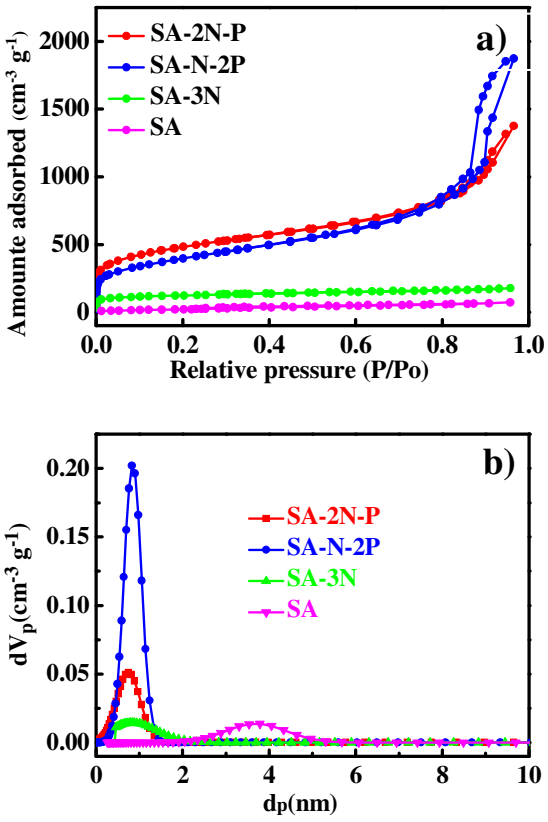

Fig. 3 (a) N_2 sorption isotherms of the samples under different activation conditions (b) Pore size distributions (PSDs) calculated from the adsorption isotherm by the non local density functional theory (NLDFT) method and assuming a slit pore model.

contribution to CO_2 adsorption than wide micropores or mesopores.[13,22] This is due to the fact that the narrow micropores have strong adsorption potentials that can enhance their filling by the CO_2 molecules. This result also tell us that the preparation of

a)

efficient CO_2 carbon sorbents requires a fine control of the porosity structure, and the micropores less than 1 nm should be ideal. In addition, it is interesting to note that among the four samples, the sample SA-2N-P possesses the highest specific surface area of 1740 $m^2 g^{-1}$, as shown in Table 1. Thus it can be seen that the binary acid can be more suitable as activating agent than the single HNO_3. All of these results suggest that the sample SA-2N-P is expected to possess the highest CO_2 adsorption capacity, which is also reasonable based on reported investigations.[13, 22]

Table 1 Textural properties of the carbons derived from SA with different activation conditions.

Samples	S_{BET} $[m^2 g^{-1}]$[a]	V_{tot} $[cm^3 g^{-1}]$[b]	d_p[nm][c]	N [wt%]
SA	103	0.11	3.78	0.63
SA-2N-P	1740	1.57	0.74	3.38
SA-N-2P	1372	1.71	0.82	1.48
SA-3N	444	0.21	0.89	1.57

[a] S_{BET} = apparent surface area calculated by the Brunauer–Emmett–Teller (BET) method. [b] Pore volume at p/p_0 = 0.99. [c] The maximum pore diameter of the PSDs calculated by NLDFT.

The X-ray photoelectron spectroscopy (XPS) technique was used to investigate the nature of the nitrogen species on the surface of the N-doped porous carbons. The status of N in the carbon materials has been well-documented and generally the nitrogen species exists in the form of highly coordinated 'pyrrolic' nitrogen or pyridine-like nitrogen incorporated into carbon matrix.[36-38] As shown in Fig. 4a-c, all the activated samples exhibit similar XPS pattern. The N1s peak can be resolved into two peaks centered at binding energies of 398.1–399.3 eV and 399.8–401.2 eV, representing pyridinic and pyrrolic nitrogen, respectively.[39] However, interestingly, compared to those of the samples SA-2N-P and SA-3N, the peaks of the samples SA-N-2P and SA occur a shift of *ca*. 1 eV, which may be ascribed to the different N contents. In our experiments, the optimum volume ratio of HNO_3 to H_3PO_4 is 2:1, and the sample SA-2N-P obtained under this condition possesses the highest N content of 3.38 %. The majority of the nitrogen comes from HNO_3 and the minority from SA itself. With decreasing the amount of HNO_3 used, the nitrogen content drops to 1.48 % for the sample SA-N-2P. As for the sample SA-3N, the HNO_3 probably reacts with the carbon precursor in the activation process, leading to evident decrease of nitrogen content. Furthermore, for the three activated samples their N content of pyrrolic type is larger than that of the pyridinic type (Fig. 4e). This is beneficial for the CO_2 capture.[11a] In contrast, the unactivated SA sample has a small content of N (0.63%) and that the content of the pyridinic N is even larger than that of the pyrrolic N (Fig. 4e). All of these results prove that the activation conditions play a key role in the nitrogen content and nitrogen species. Here, it should be noted that for SA-2N-P and SA-N-2P, besides N-doping, P element also exists in the samples in the form of PO_4^{3-} (Fig. S1), not bulk substitution, which does not contribute to the CO_2 adsorption.

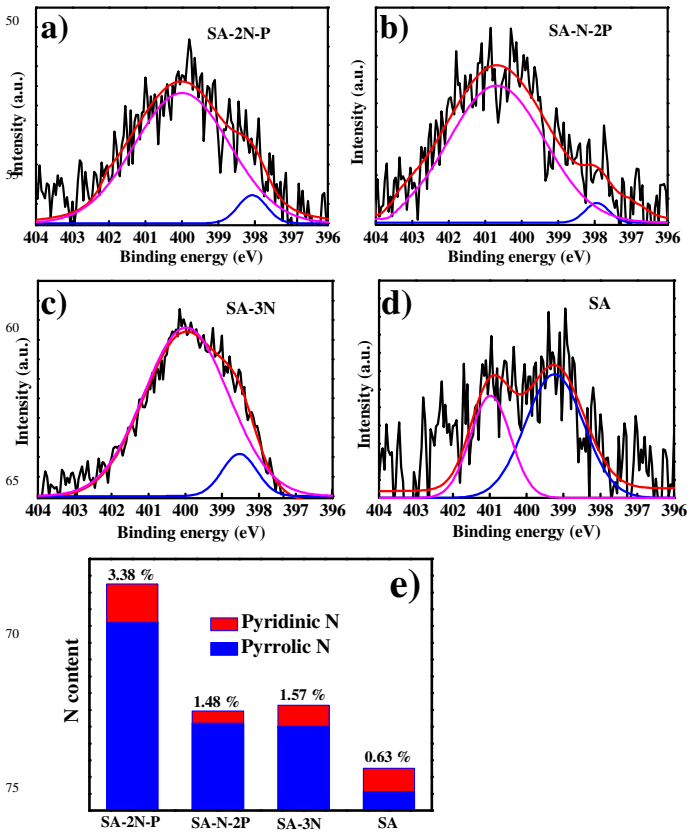

Fig. 4 N1s XPS spectra of the samples (a) SA-2N-P, (b) SA-N-2P, (c) SA-3N, (d) SA, and (e) the pyridinic N and pyrrolic N propotion comparison of the samples.

CO_2 adsorption capacity

The CO_2 adsorption capacities of above four samples were investigated at three representative temperatures (0, 25 and 45 °C) and related data are listed in Table 2. A comparative analysis of the CO_2 adsorption isotherms measured at 25 °C is presented in Fig. 5a. It can be seen that the CO_2 capture capacities of the four samples are quite substantial and distinctive. This result is coherent with the fact that the specific surface area and the nitrogen content of these materials are different (Table 1). Clearly, both surface area and the amount of N species play an important role in determining the CO_2 uptake capacity.

The sample SA-2N-P possesses the highest CO_2 adsorption capacity of 4.57 mmol g^{-1} at 298 K and 1 atm among the four samples. This value is even higher than those of other biomass-derived carbon materials. For example, Yan *et al.* prepared celtuce leaf-derived porous carbons with a CO_2 adsorption capacity of 4.36 mmol g^{-1} at 298 K and 1 atm, while Stefan *et al.* obtained fungi-based porous carbons, which showed a CO_2 adsorption capacity as low as 3.5 mmol g^{-1} at 298 K and 1 atm.[17,40] Also, compared to most of other porous materials

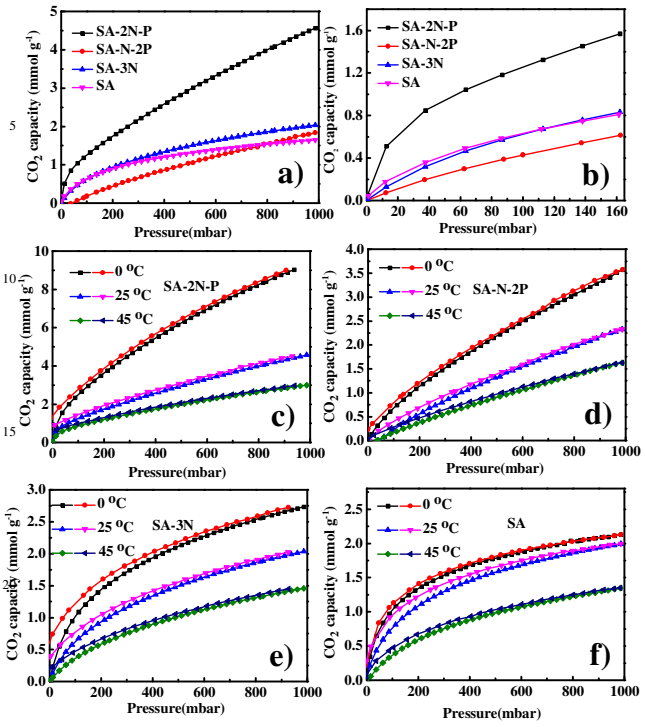

Fig. 5 (a) CO_2 adsorption isotherms at 298 K for SA-2N-P, SA-N-2P, SA-3N and SA, (b) expansion of the plots below 0.15 atm, (c)-(f) CO_2 adsorption isotherms at 0 °C, 25 °C and 45 °C for the porous carbons obtained different activation condition: (c) SA-2N-P (d) SA-N-N, (e) SA-3N, and (f) SA, respectively.

recently reported for CO_2 capture, the sample SA-2N-P demonstrates comparable and higher capacity. For example, Su *et al.* fabricated carbon nanotube modified carbon composite monoliths with the CO_2 adsorption capacity of 3.61 mmol g^{-1} (159 mg g^{-1});[10a] Myunghyun *et al.* reported a CO_2 uptake of 3.75 mmol g^{-1} (16 wt %) at ambient temperature and pressure for metal-ion-impregnated metal-organic frameworks,[4] which is higher than that of zeolite 13X (3.64 mmol g^{-1}), a promising CO_2 adsorbent.[41] What's more, the CO_2 capacity significantly increases by 99.8 % from 4.57 to 8.99 mmol g^{-1} (395.56 mg g^{-1}) for the same sample SA-2N-P when the adsorption temperature decreases from 298 to 273 K (Fig. 5c). Such an adsorption capacity is very outstanding as compared to those of previously reported adsorbents, in which the maximum value of the CO_2 adsorption capacity is 8.05 mmol g^{-1} for activated carbon spheres at 273 K and 1 atm.[42] Previous studies have shown that, at elevated activating temperatures, activated carbon has negligible CO_2-adsorption capacities due to weak chemical interactions between the carbon surface and CO_2.[43] For other three samples, they exhibit almost same CO_2 capacity (around 2 mmol g^{-1}) at 273 K and 1 atm, which is far lower than that of sample SA-2N-P. For different adsorption temperatures, these four samples all show a decreased CO_2 adsorption capacity as the temperature increases, which is well agreement with references (Fig. 5c-f). For example, the sample SA-N-2P exhibits the CO_2 capacity of 3.56 (156.64), 2.33 (102.52) and 1.62 (71.28) mmol g^{-1} (mg g^{-1}) at 0, 25 and 45 °C (1 atm), respectively.

Table 2 CO_2 capture capacities of the porous carbons at different adsorption temperatures.

Samples	CO_2 capacity/mmol g^{-1} (mg g^{-1})			
	0 °C 1 atm	25 °C 1 atm	45 °C 1 atm	25 °C 0.15 atm
SA	2.13(93.72)	1.98(87.12)	1.35(59.84)	0.95(41.8)
SA-2N-P	8.99(395.56)	4.57(201.08	2.98(131.12)	1.51(66.44)
SA-N-2P	3.56(156.64)	2.33(102.52)	1.62(71.28)	0.58(25.52)
SA-3N	2.73(120.12)	2.02(88.88)	1.45(63.8)	0.79(34.76)

From above results, SA-2N-P really displays a good property for CO_2 capture, which is closely associated with its physical properties. From Table 1, we know that among all samples, the sample SA-2N-P has the highest specific surface area of 1740 m^2 g^{-1}, which is mainly due to the presence of a large number of narrow micropores (<1 nm). In addition, its nitrogen content (3.38 %) is also the highest among all samples, and that its pyrrolic nitrogen content is far higher than those of the other three samples. It has been documented that pyrrolic nitrogen generally has much more contribution for CO_2 capture than pyrdinic nitrogen.[11a,44] Covalently tethered nitrogen functional groups are believed to be Lewis-base active sites for binding the acidic CO_2.[45,46] For sample SA-N-2P, although it possesses the specific surface area as high as 1372 m^2 g^{-1}, the nitrogen content (1.48 %) is relatively low, leading to its low CO_2 adsorption capacity, whereas for the un-activated SA sample, its specific surface area is significantly lower than those activated samples, and therefore its low CO_2 adsorption capacity is reasonable. Furthermore, for the sample SA-3N, its CO_2 capacity is low, which is also consistent with its textural property of low specific surface area. Thus it can be deduced that too much HNO_3 leads to excessive activation, which destroys the pores. From above analysis, it can be concluded that the higher surface area and pyrrolic nitrogen content are responsible for the high CO_2 adsorption capacity for the sample SA-2N-P. In addition, the CO_2 adsorption capacities of the four samples are much higher than that (0.89 mmol g^{-1}) of the commercial activated carbon.[47.]

From practical aspect, the concentration of CO_2 from the flue gas is only 10–15% CO_2, which is extremely low and unfavorable on CCS. It is also noteworthy that the sample SA-2N-P displays outstanding CO_2 adsorption capacity of 1.51 (66.44) mmol g^{-1} (mg g^{-1}) at 150 mbar and 298 K in Fig. 5b. This value is higher than the reference value (52 mg g^{-1}) at the same conditions.[10] Therefore, the sample SA-2N-P could used as a promising CO_2 adsorbent.

CO_2/N_2 selectivity

Besides the high CO_2 uptake, the adsorption capacity of SA-2N-P for N_2 is also measured under the same experimental conditions. As shown in Fig. 6a, the adsorption capacity of N_2 is much lower than that of CO_2 for the same sample, reaching a maximum of 0.60 mmol g^{-1} at 298 K and 1 atm. Thus, at identical pressure for both CO_2 and N_2, the amount of N_2 adsorbed is only one seventh that of CO_2. Therefore, SA-2N-P, could be a potential selective adsorbent for CO_2 and N_2 separation.

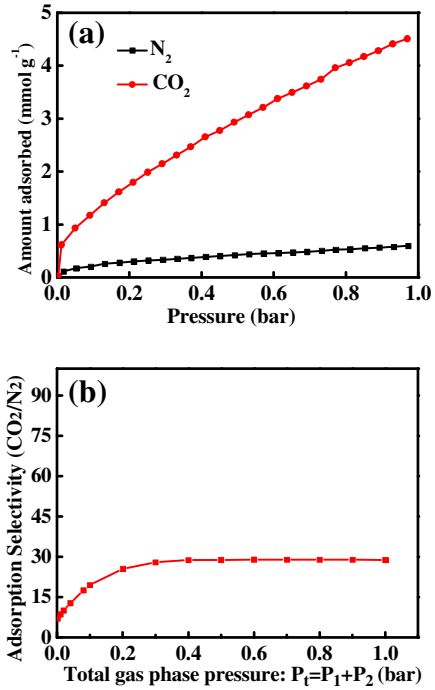

Fig. 6 (a) Adsorption curves of the sample SA-2N-P at 298 K in a N_2 and CO_2 atmosphere and (b) IAST-predicted adsorption selectivity for binary mixture of 15:85 CO_2/N_2 at 298 K and 1 atm.

The ideal adsorption solution theory (IAST) of Myers and Prausnitz has been reported to predict binary gas mixture adsorption in many porous materials accurately.[48] The absolute component loadings were fitted with a dual-site Langmuir model. (Fig. S2). To evaluate the merit of the sample SA-2N-P for CO_2/N_2 separation, the adsorption selectivity, S_{ads}, for binary mixturesof CO_2 and $\mathbf{N_2}$, is defined as follows:[7,12,48]

$$S_{ads} = \frac{q_1 / q_2}{p_1 / p_2} \quad (1)$$

where q_i is the amount of i adsorbed and p_i is the partial pressure of i in the mixture for CO_2 over N_2 in flue-gas streams (typically 15% CO_2 and 85% N_2). The SA-2N-P exhibits high adsorption selectivity of 29 for CO_2 over N_2 at 299 K and 1 atm (Fig. 6b). This result indicates that CO_2 and N_2 can be successfully separated by SA-based carbon materials. Therefore, the sample SA-2N-P can be considered as a promising absorbent and further application of novel SA-based carbon materials are currently being investigated.

CO_2 adsorption and isosteric heat of adsorption (Q_{st})

Isosteric analysis of adsorption isotherms collected at various temperatures allows an estimation of the coverage-dependent isosteric heat of adsorption (Q_{st}), where the behavior of this function is determined by the relative magnitudes of the adsorbent-adsorbate and adsorbate-adsorbate interactions. To better understand the adsorption properties, the isosteric heats of adsorption (Q_{st}) were calculated from:

$$Q_{st} = RT^2 \left(\frac{\partial \ln p}{\partial T} \right)_q \quad (2)$$

The details of the analytic procedure adopted for determining Q_{st} using the dual-site Langmuir model are based on previous reports.[7a,49] As shown in Fig. 7, the isosteric heats of CO_2 adsorption loading on the four samples are between 20 and 43 kJ mol^{-1}. The sample SA-2N-P possesses the highest Q_{st} of 43 kJ mol^{-1}, and this result is consistent with its high selectivity of CO_2 over N_2. Compared to other solid absorbents, this value is considerable brilliant. For example, at 1 mmol g^{-1} loading the isosteric heat of CO_2 adsorption of silicalite is 28 kJ mol^{-1}.[50,51] For common MOFs, their isosteric heats of CO_2 adsorption are in the range of 25–35 kJ mol^{-1}.[4] Antonio *et al.* have prepared N-doped porous carbon materials with the Q_{st} of 31.5 kJ mol^{-1} at 0.6 mmol g^{-1} CO_2 uptake.[11a]

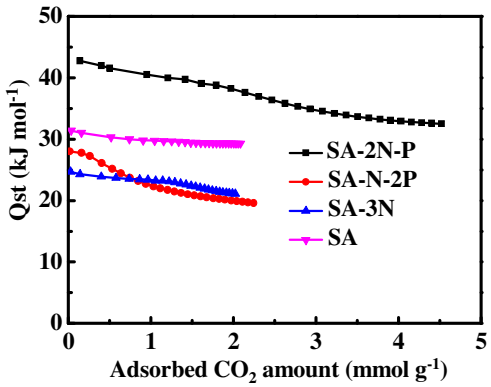

Fig. 7 Isosteric heats of adsorption Q_{st} for the adsorption of CO_2, calculated using the dual-site Langmuir isotherm fits.

4. Conclusions

In summary, we prepared a series of highly porous carbon materials by using the binary mixture of H_3PO_4-HNO_3 as a co-activating agent for the first time. Interestingly, SA, which has been considered as a waste from the point of view of biofuel production, can be used as a very attractive carbon source in our study. It is worthy to note that the binary acid mixture of H_3PO_4-HNO_3 as a co-activating agent becomes a new member for the chemical activation family. These activated carbons possess high specific surface area and exhibit a high efficiency for CO_2 capture. Particularly, the as-obtained sample SA-2N-P exhibits the highest CO_2 adsorption capacity of 8.99 mmol g^{-1} at 273 K and 4.57 mmol g^{-1} at 298 K (1 atm). The high capacity of CO_2 adsorption is due to the presence of narrow micropores (<1 nm) and high nitrogen doping. Furthermore, the sample SA-2N-P exhibits a good selectivity for CO_2/N_2 separation and has high initial and average CO_2 adsorption energy (Q_{st}) of 43 and 30 kJ mol^{-1}, respectively. Considering these merits, the sample can be used as a promising material for CO_2 capture and storage.

Acknowledgements

This work was financially supported by the National Natural Science Foundation of China 21173021, 21231002, 21276026, 21271023, 91022006, and 20973023, the 111 Project (B07012), 973 Program (2014CB932103).

References

1. M. Nandi, K. Okada, A. Dutta, A. Bhaumik, J. Maruyama, D. Derksa

and H. Uyama, *Chem. Commun.*, 2012, **48**, 10283.
2. D. M. D-Alessandro, B. Smit, and J. R. Long, *Angew. Chem. Int. Ed.,* 2010, **49**, 6058.
3. IPCC, IPCC Special Report on Carbon Dioxide Capture and Storage, *Cambridge University Press*, Cambridge, 2005.
4. a) H. J. Park and M. P. Suh, *Chem. Sci.*, 2013, **4**, 685; b) X. L. Si, C. L. Jiao, F. Li, J. Zhang, S. Wang, S. Liu, Z. B. Li, L. X. Sun, F. Xu, Z. Gabelicad and C. Schick, *Energy Environ. Sci.*, 2011, **4**, 4522.
5. a) K. Sumida, D. L. Rogow, J. A. Mason, T. M. McDonald, E. D. Bloch, Z. R. Herm, T. H. Bae and J. R. Long, *Chem. Rev*., 2012, **112**, 724; b) P. Nugent, Y. Belmabkhout, S. D. Burd, A. J. Cairns, R. Luebke, K. Forrest, Tony Pham, S. Q. Ma, B. Space, L. Wojtas, M. Eddaoudi and M. J. Zaworotko, *Nature*, 2013, **495**, 80.
6. a) H. S. Choi and M. P. Suh, *Angew. Chem. Int. Ed.,* 2009, **48**, 6865; b) C. Xu and N. Hedin, *J. Mater. Chem. A*, 2013, **1**, 3406.
7. a) W. G. Lu, J. P. Sculley, D. Q. Yuan, R. Krishna, Z. W. Wei, and H. C. Zhou, *Angew. Chem., Int. Ed.*, 2012, **51**, 7480; b) W. G. Lu, D. Q. Yuan, J. Sculley, D. Zhao, R. Krishna and H. C. Zhou, *J. Am. Chem. Soc.*, 2011, **133**, 18126.
8. F. S. Su and C. Y. Lu, *Energy Environ. Sci.*, 2012, **5**, 9021.
9. F. Akhtar, Q. L Liu, N. Hedinab and L. Bergstr, *Energy Environ. Sci.,* 2012, **5**, 7664.
10. a) Y. G. Jin, S. C. Hawkins, C. P. Huynhb and S. Su, *Energy Environ. Sci.,* 2013, **6**, 2591; b) W. Xing, C Liu, Z. Y. Zhou, L Zhang, J Zhou, S. P. Zhuo, Z. F. Yan, H. Gao, G. Q. Wang and S. Z. Qiao, *Energy Environ. Sci.*, 2012, **5**, 7323; c) L. Zhao, Z. Bacsik, N. Hedin, W. Wei, Y. H. Sun, M. Antonietti and M. M. Titirici, *ChemSusChem*, 2010, **3**, 840.
11. a) M. Sevilla, P. Valle-Vigon and A. B. Fuertes, *Adv. Funct. Mater.*, 2011, **21**, 2781; b) A. Wahby, J. M. Ramos-Fernández, M. Martínez-Escandell, A. Sepúlveda-Escribano, J. Silvestre-Albero and Francisco Rodríguez-Reinoso, *ChemSusChem*, 2010, **3**, 974; c) V. Presser, J. McDonough, S.-H. Yeon and Y. Gogotsi, *Energy Environ. Sci.*, 2011, **4**, 3059.
12. a) Y. F. Zhao, L. Zhao, K. X. Yao, Y. Yang, Q. Zhang and Y. Han, *J. Mater. Chem.*, 2012, **22**, 19726; b) Y. F. Zhao, X. Liu, K. X. Yao, L. Zhao and Y. Han, *Chem. Mater.*, 2012, **24**, 4725.
13. a) Y. M. Zhang, B. Y. Li, K. Williams, W. Y. Gao and S. Q. Ma, *Chem. Commun.* 2013, **49**, 10269; b) Y. Q. Li, T. Ben, B. Y. Zhang, Y. Fu and S. L Qiu, *Scientific Reports*, Doi:10.1038/srep02420.
14. S. Cui, W. W. Cheng, X. D. Shen, M. H. Fan, A. (Ted) Russell, Z. W. Wu and X. B. Yi, *Energy Environ. Sci.*, 2011, **4**, 2070.
15. J. H. Drese, S. Choi, R. Lively, M. Gray, D. J. Fauth, C. W. Jones, *Adv. Funct. Mater*. 2009, **19**, 3821.
16. H. Zhu, X. L. Wang, F. Yang, X. R. Yang, *Adv. Mater.* 2011, **23**, 2745.
17. R. T. Wang, P. Y. Wang, X. B. Yan, J. W. Lang, C. Peng and Q. J. Xue, *Appl. Mater. Interfaces*, 2012, **4**, 5800.
18. L. Wei, M. Sevilla, A. B. Fuertesm, R. Mokaya, G. Yushin, *Adv. Energy Mater.*, 2011, **1**, 356.
19. R. T. Wang, P. Y. Wang, X. B. Yan, J. W. Lang, C. Peng and Q. J. Xue, *J. Phys. Chem. C,* 2012, **116**, 1099.
20. T. Horikawa, N. Sakao, T. Sekida, J. Hayashi, D. D. Do, M. Katoh, *Carbon,* 2012, **50**, 1833.
21. J. Górka, M. Jaroniec, *Carbon*, 2011, **49**, 154.
22. M. Sevilla and A. B. Fuertes, *Energy Environ. Sci.*, 2011, **4**, 1765.
23. Z. R. Yue, R. Kelly Benak, J. W. Wang, C. L. Mangunb and J. Economy, *J. Mater. Chem.*, 2005, **15**, 3142.
24. M. B. Vázquez-Santos, F. Suárez-García, A. Martínez-Alonso, and J. M. D. Tascón，*Langmuir*, 2012, **28**, 5850.
25. P. J. Walsh, X. Hu, P. Cunniff, A. J. Lesser, *J. Appl. Polym. Sci.* 2006, **102**, 3517.
26. Y. H. So, S. J. Martin, K. Owen, P. B. Smith, C. L. Karas, *J. Polym. Sci., Part. A: Polym. Chem.* 1999, **37**, 2637.
27. T. M. Richard, F. F. Pasquale, Z. Ma and S. Dai, *Phys. Chem. Chem. Phys*., 2011, **13**, 2492.
28. X. L. Wu, W. Wang, Y. G. Guo and L. J Wan, *Journal of Nanoscience and Nanotechnology*, 2011, **11**, 1897.
29. P. X. Han, Y. H. Yue, L. X. Zhang, H. X. Xu, Z. H Liu, K. J. Zhang, C. J Zhang, S. M Dong, W. Ma, G. L. Cui, *Carbon*, 2012, **50** 1355.
30. W. F. Chen, L. F. Yan, P. R. Bangal, *Carbon*, 2010, **48**, 1146.
31. J. F. Shen, Y. Z. Hu, M. Shi, X. Lu, C. Qin, C. Li and M. X. Ye, *Chem. Mater.*, 2009, **21**, 3514.
32. A. C. Ferrari and J. Robertson, *Physical review B*, 2000, **61**, 14095.
33. L. F. Qi, J. G. Yu and M. Jaroniec, *Phys. Chem. Chem. Phys.*, 2011, **13**, 8915.
34. K. S. W. Sing, D. H. Everett, R. A. W. Haul, L. Moscou, R. A. Pierotti, J. Rouquerol and T. Siemieniewska, *Pure Appl. Chem.*, 1985, **57**, 603.
35. M. Kruk and M. Jaroniec, *Chem. Mater.*, 2001, **13**, 3169.
36. Y. D. Xia , G. S. Walker , D. M. Grant , R. Mokaya , *J. Am. Chem. Soc.*, 2009 , **131** , 16493.
37. Z. X. Yang, Y. D. Xia, R. Mokaya, *J. Am. Chem. Soc.*, 2007, **129**, 1673.
38. Y. D. Xia, R. Mokaya, G. S. Walker and Y. Q. Zhu, *Adv. Energy Mater.*, 2011, **1**, 678.
39. H. Wang, T. Maiyalagan and X. Wang, *ACS Catal.,* 2012, **2**, 781.
40. J. C. Wang, A. Heerwig, M. R. Lohe, M. Oschatz, L. Borchardt and S. Kaskel, *J. Mater. Chem.*, 2012, **22**, 13911.
41. R. V. Siriwardane, M. S. Shen, E. P. Fisher, J. A. Poston, *Energy Fuels*, 2001, **15**, 279.
42. P. N. Wickramaratne and M. Jaroniec, *ACS Appl. Mater. Interfaces*, 2013, **5**, 1849.
43. N. D. Hutson, *Chem. Mater.* 2004, **16**, 4135.
44. J. R. Pels, F. Kapteijn, J. A. Moulijn, Q. Zhu, K. M. Thomas. *Carbon*, 1995, **33**, 1641.
45. G. P. Hao, W. C. Li, D. Qian and A. H. Lu, *Adv. Mater*. 2010, **22**, 853.
46. M. D. Soutullo, C. I. Odom, B. F. Wicker, C. N. Henderson, A. C. Stenson, J. H. Davis, *Chem. Mater*. 2007, **19**, 3581.
47. M. M. Maroto-Valer, Z. Tang and Y. Zhang, *Fuel Process. Technol.*, 2005, **86**, 1487.
48. A. L. Myers, J. M. Prausnitz, *AICHE J*. 1965, **11**, 121
49. J. A. Mason, K. Sumida, Z. R. Herm, R. Krishna, J. R. Long, *Energy Environ.Sci.* **2011**, *4*, 3030.
50. M. S. Fallah, A. Rothenberger, A. P. Katsoulidis, J. Q. He, C. D. Malliakas and M. G. Kanatzidis, *Adv. Mater.* 2011, **23**, 4857.
51. J. A. Dunne , R. Mariwals , M. Rao , S. Sircar , R. J. Gorte , A. L. Myers ,*Langmuir,* 1996, **12**, 5888.